Effect of Material Elasticity on the Longitudinal AC Breakdown Strength of Solid-Solid Interfaces

Emre Kantar and **Erling Ildstad**
Department of Electric Power Engineering
Norwegian University of Science and Technology
Trondheim, 7491, Norway

Sverre Hvidsten
Department of Electric Power Technology
SINTEF Energy Research
Trondheim, 7465, Norway

ABSTRACT

Solid-solid interfaces between insulating materials dictate the long-term electrical properties of the complete insulation system. This paper presents theoretical and experimental investigations aiming to address the impact of the material elasticity on tangential AC breakdown strength (BDS) of interfaces between polymers. Four different polymers with different elastic moduli were tested using: Cross-linked polyethylene (XLPE), filled epoxy resin (EPOXY), polyether ether ketone (PEEK) and silicone rubber (SiR). The interfaces were formed between identical specimens and were breakdown tested at various contact pressures. It was found that elastic modulus and contact pressure had pronounced effects on the BDS of interfaces. Higher elastic modulus correlated with decreased BDS by a factor of 1.6 at the same contact pressure. On the other hand, the increase of contact pressure by a factor of 3 elevated the interfacial BDS by a factor of 1.4 in the case of the lowest elastic modulus (SiR-SiR) whereas that for the highest modulus (PEEK-PEEK) was about 2.4 times higher. Using the proposed theoretical approach, we postulated that discharged cavities govern the interfacial BDS at the interface together with the electrical tracking resistance of contact area between the cavities. Although the electrical tracking resistance increases with a higher modulus, local field enhancements due to discharged cavities also increase significantly. Therefore, the observed reduction of the BDS with the increase of the elastic modulus is ascribed to the larger cavity size and hence the smaller contact area. It is concluded that increased elasticity reduces the dominance of the discharged cavities over the interface breakdown and increase the governance of the electrical tracking resistance of the contact spots.

Index Terms — **breakdown, cable connector, cable joint, dielectric, interface, electrical tracking resistance, interfacial discharge, roughness, surface breakdown**

1 INTRODUCTION

SUBSEA cable connectors are vital components of oil and gas installations, future offshore wind and wave energy systems. Although materials and production technologies for subsea applications have shown a good service experience over the years, cable connectors and joints are still considered the weaker parts of complete cable systems [1, 2].

One of the leading causes of the electrical weakness is the existence of solid-solid interfaces in cable apparatus and joints [1]. An interface contains microscopic imperfections such as cavities, protrusions, and contaminants that can reduce the tangential AC electric breakdown strength (BDS) of the interface since these imperfections cause local electric field enhancements [3]. Local fields are likely to initiate partial discharges (PD) and trigger field enchancements that can lead to tracking failure eventually [4, 5]. Studies of insulating materials for cables and accessories have been covered extensively in the literature. The interfacial breakdown (BD) between the contacting surfaces of two dielectric materials was reported to represent one of the principal causes of failure for power cable joints and connectors, where elastic modulus plays a critical role [4-7]. Under varying interfacial pressures, the elastic modulus has a significant influence on the structure of the cavities at the interfaces [8], and hence on the BDS of the interface [9]. There is, however, lack of a clear correlation between the elastic modulus and the BDS of the polymer interfaces. With the motivation of filling in this research gap, the effect of the elastic modulus on the tangential AC breakdown strength of dry-assembled interfaces between polymers under various interfacial contact pressures is analytically and experimentally studied herein.

In the experiments, AC breakdown testing of solid-solid interfaces was carried out, where four different interfaces between polymers with different elastic moduli were subjected to various contact pressures. The theoretical hypothesis is built on an extensive contact surface model developed in [9] to verify the trends observed in the experiments and to conjecture on the possible mechanisms controlling the interfacial breakdown phenomenon. Some of the breakdown experiments were repeated for PD testing of the interfaces to test the validity of the proposed hypothesis.

Manuscript received on 01 April 2018, in final form 15 June 2018, accepted 21 July 2018. Corresponding author: E. Kantar.

This is the accepted version of an article published in IEEE transactions on dielectrics and electrical insulation
DOI: 10.1109/TDEI.2019.008087

2 BACKGROUND AND THEORY

When two nominally flat solid surfaces are assembled, contacts occur at discrete spots that lead to numerous cavities between surface asperities at the interface [8]. An interface hence consists of strings of cavities and contact spots linked to each other as illustrated in Figure 1.

Shape, size, and number of cavities and contact spots determine the breakdown strength of an interface. Since the dielectric strength of a gas-filled cavity is much lower than that of bulk insulation, cavities are one of the weakest parts of the interface against electrical breakdown [2]. Thereby, PD activity presumably begins in the cavities first [10]. The discharged cavities, however, do not necessarily lead to the breakdown of the contact spots immediately. The electrical tracking resistance of the insulation determines the withstanding ability of the contact spots against interfacial discharge [4-7]. In the interface breakdown model, the cavity discharge and PD resistance will be correlated with the interfacial breakdown.

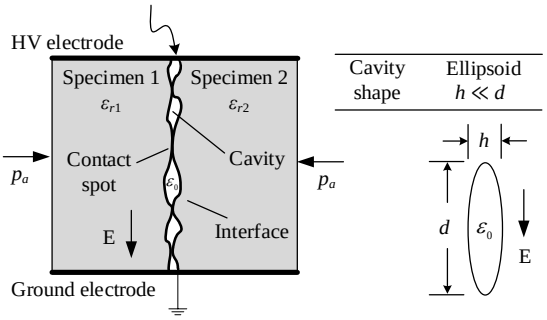

Figure 1. An illustration of the air-filled cavities (ε_0 therein) at the interface in a two-dimensional profile.

2.1 MODELING OF AVERAGE SIZE AND SHAPE OF CAVITIES AND CONTACT SPOTS

The tribological contact surface model developed in [9] is used to estimate the average size of the cavities and the contact spots. The contact model initially requires real surface texture profiles of the materials and then transforms two rough surfaces into one equivalent rough surface and a smooth plane as explained in [9]. In essence, in a 2-D plane, cavities formed at the interface can be approximated with an ellipsoid whose length parallel to the electric field (d) is approximately 8–9 times larger than the length normal to the field (h) as shown in Figure 1. For such a cavity, the correlation between the interfacial contact pressure p_a, the elastic modulus E, and the average length of cavities d_{avg} is given by [9]:

$$d_{avg} = \frac{2\left(E'\sqrt{\frac{\sigma_p}{\beta_m}} - 3.2p_a\right)^{0.5} \beta_m^{0.47}\sigma_p^{0.41}}{\sqrt{1.21\pi}E'^{0.06}\eta^{0.06}p_a^{0.44}}, \quad (1)$$

where E' is the effective elastic modulus of two materials in contact, σ_p is the standard deviation of the asperities' heights, β_m is the mean radius of the asperities' summit, and η is the surface density of asperities [8, 9]. The surface parameters η, β_m and σ_p need to be computed using measured real surface roughness profiles to calculate d_{avg}.

A similar approach is performed to derive the average length of the contact spot l_{avg} in series with the cavities:

$$n = 1.21\eta A_a\left(\frac{p_a}{\eta\sigma_p\beta_m E'\sqrt{\sigma_p/\beta_m}}\right)^{0.88}, \quad (2)$$

$$A_{re} = \sum_{j=1}^{n} A_{cnt,j} = n\pi\left(\frac{l_{avg}}{2}\right)^2, \quad (3a)$$

$$l_{avg} = 2\sqrt{\frac{A_{re}}{n\pi}} = 1.84\frac{\beta_m^{0.47}\sigma_p^{0.41}p_a^{0.06}}{E'^{0.06}\eta^{0.06}}, \quad (3b)$$

where n is the number of cavity and contact spot pairs, A_{re} is the total real area of contact, A_a is the nominal contact area and $A_{cnt,j}$ stands for the respective area of the j^{th} contact spot. When deriving l_{avg}, number of contact spots is assumed equal to the number of cavities, and the contacting areas are assumed spherical [9]. As seen, the model suggests that d_{avg} decreases as E' is increased that in turn reduce l_{avg}.

2.2 ESTIMATION OF CAVITY DISCHARGE INCEPTION FIELD

The electric field at which the BDS of the gas in the cavity is exceeded is defined as cavity discharge inception field or partial discharge inception field (CDIE). Under a homogeneous electric field, the CDIE of an air-filled cavity can be characterized in the form of a Paschen curve, which could be represented by a polynomial fit with the form [2]:

$$\mathrm{CDIE}\,(p_c, d) = A\frac{p_0/p_c}{d^2} + B\left(p_c/p_0\right) + \frac{C}{d} + D\sqrt{\frac{p_c/p_0}{d}}, \quad (4)$$

where p_c is the pressure inside of the cavity, and p_0 = 1 bar, A = 0.00101 kV·mm, B = 2.4 kV/mm, C = − 0.0097 kV, D = 2.244 kV·mm$^{-0.5}$ [2].

Since any direction of the field within the ellipsoid can be resolved into three orthogonal components, it is sufficient to consider the axis parallel to the field since the minimum value of CDIE is associated with the maximum path length in the field direction (critical avalanche length) [10]. Thus, the average length of the cavities in the direction of the applied field d_{avg} is substituted for d in Equation (4). Depending on the elasticity and contact pressure, cavities can either be trapped or form larger cavities or channels by connecting with other cavities at the interface. In the case of large cavities or channels, initially compressed air is assumed to be squeezed out and is vented to the surroundings. According to Paschen's law; however, the CDIE of vented cavities, in which the gas pressure settles around the ambient pressure ($p_c \approx 1$ bar), is much lower than that of interlocked cavities with p_c greater than 1 bar. Consequently, the vented cavities are assumed to dominate the CDIE, and PD activity starts in a cavity whose length parallel to the electric field is equal to or greater than d_{avg}, whereas there is presumably no discharge activity in smaller cavities.

2.3 ESTIMATION OF PD RESISTANCE AND MODELING OF ENHANCED LOCAL FIELDS

As Illias et al. [10] reported in their respective studies, strong non-homogeneous local fields occur at the edges of the discharged cavities enclosed by contact spots despite the

This is the accepted version of an article published in IEEE transactions on dielectrics and electrical insulation
DOI: 10.1109/TDEI.2019.008087

uniform electric field (see Figure 2). The field reduces considerably (i.e., short-circuited) in a discharged cavity until the discharge is quenched whereas it is at the rated value in the bulk insulation as illustrated in Figure 2. Whether the resulting local field spikes (due to discharges in the cavities) can cause a complete flashover (i.e., interfacial discharge) across the interface strongly depend upon the electrical tracking resistance of the insulation [5-7].

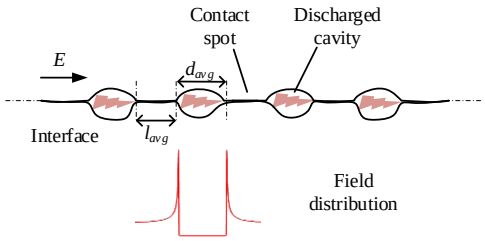

Figure 2. An illustration of the field lines at the interface in 2-D profile from the finite-element analysis performed. The dimensions of the defined cavities are so small that the internal field is deemed effectively uniform [10].

We assume that the local enhanced fields at edges of contact spots can be emulated by a needle-plane or a needle-needle electrode configuration. The crest values of the field can then be estimated via empirical models as if they are caused by the needle tips. Subsequently, the electrical tracking resistance of the contact spots can be checked if the contact spots could withstand the local field spikes or an interfacial discharge would occur.

The field strength at the tip of a needle is a few orders of magnitude higher than the estimated intrinsic BDS of polymers [7]. The enhanced field at the edges of a discharged cavity emulated with a needle-needle geometry can be estimated by:

$$E_{enh} = \frac{V_{app}\sqrt{1+r_n/l}}{r_n \operatorname{arctanh}\left(\sqrt{1+r_n/l}\right)^{-1}}, \quad (5)$$

where r_n is the radius of the tip of the needle, V_{app} is the applied voltage, l is the distance between the electrodes [7]. When calculating E_{enh}, the average length of contact spots l_{avg} is used for l, i.e. $l = l_{avg}$.

Needle-plane type experimental configurations with different needle tip radii were extensively used in the literature to examine electrical tracking resistance of insulation materials under AC, DC or impulse [5-7]. Using empirical data, Fothergill [6] developed the following expression to estimate the electrical tracking resistance E_{tr}:

$$E_{tr} = \left(\frac{16 G E'}{\varepsilon_0^2 \varepsilon_r^2 r}\right)^{1/4}, \quad (6)$$

where the toughness G is a constant in J/m^2, E' is Young's/elastic modulus in Pa, ε_0 is the permittivity of vacuum in F/m, ε_r is the relative permittivity of the dielectric medium, and r is the radius of the main tubular branch of the breakdown channel in m [6]. The mechanism proposed here is operative at higher local electric fields and is a breakdown rather than an aging mechanism that predicts a breakdown time of $\lesssim 10^{-7}$ s from the initiation of tracking to a flashover [6]. Therefore, Equation (6) does not incorporate time as a parameter.

The value of radius r depends on the agent initiating the filament; such as a microvoid, an impurity particle, an electrode irregularity, an electrical tree, or a feature of the polymer morphology and is assumed constant in a specimen [6]. In our model, we assume that the radius of the BD channel is equal to the radius of the needle tip, i.e., $r = r_n$.

2.4 INTERFACE BREAKDOWN MODEL

The modeled mechanisms of the cavity discharge and the breakdown of contact spots are enabled in a sequence at two different instants that trigger these mechanisms. Firstly, the inception of the cavity discharge is represented by 'instant I' in Figure 3, before which presumably no discharge activity occurs at the interface. Until 'instant II,' the contact spots endure the enhanced local fields across them, and in case the electrical tracking resistance of the insulation is exceeded (at the instant II), the breakdown of the contact spots takes place that bridges the electrodes.

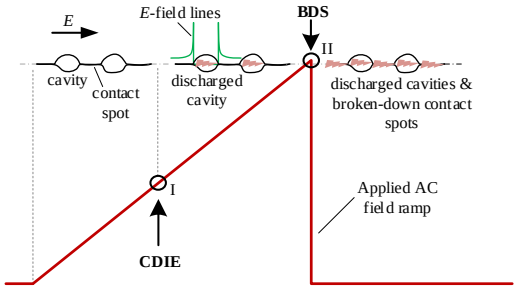

Figure 3. Modeled mechanisms of the cavity discharge and the breakdown of contact spots in parallel with applied field ramp.

In the discussion, first, estimated CDIE values by Equation (4) are associated with the experimentally obtained BDS. Next, E_{enh} is calculated separately at the instants I and II. The resulting enhanced fields are then compared with the PD resistances E_{tr} to assess if the contact spots could withstand the intense field at their edges, or interfacial discharge is likely to occur.

3 EXPERIMENTAL METHODOLOGY

3.1 SET-UP FOR AC BREAKDOWN TESTS

A simple illustration of the test set-up with the dimensions of the core components is shown in Figure 4. Two rectangular prism-shaped samples (55 mm x 30 mm x 4 mm) are assembled between two Rogowski-type electrodes under dry conditions. The electrical breakdown strength was measured by applying an AC (50 Hz) voltage ramp of 1 kV/s until BD occurred.

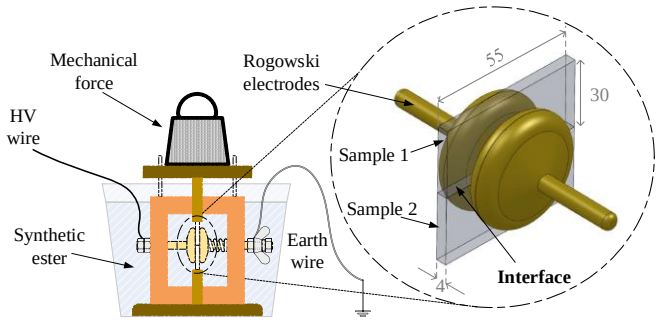

Figure 4. Illustration of the test set-up. All dimensions are in mm, electrode diameter = 40 mm. The interface is 4−mm, parallel to the direction of the field.

This is the accepted version of an article published in IEEE transactions on dielectrics and electrical insulation
DOI: 10.1109/TDEI.2019.008087

3.2 PREPARATION OF THE SAMPLES

We used four different polymers, namely silicone rubber (SiR), cross-linked polyethylene (XLPE), filled epoxy resin (EPOXY), and polyether ether ketone (PEEK). Source materials and methods to prepare each sample in the desired dimensions are shown in Table 1. *Casting* refers to the polymers we molded and cast in our laboratories whereas *cutting* stands for re-dimensioning from the bulk.

Table 1. Polymers used in this study.

Polymer	Source	Method
SiR	Liquid silicone rubber	Casting
XLPE	145 kV power cable	Cutting
EPOXY	Al-filled epoxy resin	Casting
PEEK	High-viscosity, unreinforced PEEK	Cutting

Interfaces between identical materials were tested (i.e., XLPE-XLPE, SiR-SiR, etc.) throughout this study because interfaces between different materials add more complexity to the interpretation of results due to the variation of electrical properties in addition to the modulus. The contact surfaces of the samples were polished using a grinding machine. Only grit #500-type sandpaper was used when polishing the surfaces. SiR samples were sandwiched between XLPE samples when grinding since SiR is somewhat soft, which made attaining an unstrained surface contact challenging when not sandwiched by a harder material [11].

3.3 TEST PROCEDURE AND DATA PROCESSING

The desired contact pressure was exerted using weights varying between 3−75 kg to press the samples vertically against one another. The average contact pressure is then calculated using the nominal contact area of $A_a = 220 \cdot 10^{-6}$ m^2. The applied pressure levels were determined via preliminary tests, where the samples and the interface were checked against deformation and ester penetration. For instance, the XLPE interface could not be tested above 16.7 bar due to deformation of the samples. Likewise, the SiR samples deforming beyond 2.7 bar prevented them from having been tested at higher contact pressures.

All the breakdown tests were performed with the set-up submerged in a container filled with synthetic ester oil to prevent any external flashover. To avoid ester from penetrating the interface, we applied the contact pressure before filling the container with the ester. The interface was tested against ester penetration before [11].

For each interface at each contact pressure, eight measurements were performed using a virgin pair of samples every time. The obtained results were statistically assessed using the two-parameter Weibull distribution. For further evaluation, the nominal value of the Weibull (i.e., 63.2%) with the 90% confidence interval (CI) was employed. Goodness-of-fit in each case was tested [11].

3.4 ELASTIC MODULUS MEASUREMENT

Elastic moduli of the SiR, XLPE, EPOXY, and PEEK were measured using tensile testing using *LloydLR5K* gauge following the ASTM D 790 standard. Five measurements for each material were carried out using dog bone-shaped samples. Compression testing also provided similar results [11].

The slope of the applied force (stress) to the elongation of the specimen (strain) curve in the initial linear region is constant and stands for the elastic modulus E. The effective elastic moduli E' of the assembled surfaces are calculated using the following relation:

$$\frac{1}{E'} = \frac{1}{2}\left(\frac{1-\nu_1^2}{E_1} + \frac{1-\nu_2^2}{E_2} \right), \tag{7}$$

where E_1, ν_1, and E_2, ν_2 are the elastic modulus and Poisson's ratio of each material in contact, respectively [9].

3.5 SURFACE ROUGHNESS CHARACTERIZATION

A 3D-optical profilometer (*Bruker Contour GT−K*) was used to scan the surface texture of the samples. The magnification was 50X with 0.2 µm lateral sampling resolution and 3 nm vertical resolution. The scanned surface area was 125 µm x 95 µm. Several scans were performed at different sections to examine consistency.

4 RESULTS

4.1 ELASTIC MODULUS MEASUREMENT

Table 2 displays the calculated elastic moduli E using the performed stress vs. strain measurement for each material and the resulting effective moduli E'. The results indicate that the harder the material, the higher the elastic modulus.

Table 2. Elastic moduli of samples and effective modulus of interfaces.

Interface	E_1 [MPa]	ν_1	E_2 [MPa]	ν_2	E' [MPa]
SiR−SiR	59	0.48	59	0.48	109
XLPE−XLPE	200	0.46	200	0.46	226
EPOXY−EPOXY	4425	0.38	4425	0.38	5166
PEEK−PEEK	7515	0.38	7515	0.38	8808

4.2 SURFACE ROUGHNESS PARAMETERS

Figure 5 presents roughness and waviness profiles of the polished surface of a specimen. Using the measured roughness and waviness profiles, the surface roughness parameters η, β_m and σ_p were computed by following the procedure in [9]. The parameters shown in Table 3 are substituted in Equations (1) and (3b) to calculate d_{avg} and l_{avg}.

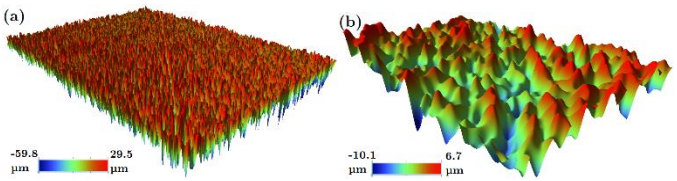

Figure 5. 3D XLPE surface profiles ground by #500: (a) Roughness profile. (b) Waviness profile.

Table 3. Surface characterization parameters.

Interface	σ_p [µm]	β_m [µm]	η [µm]
SiR	1.07	20.39	$1.6 \cdot 10^{15}$
XLPE	2.55	6.39	$2.8 \cdot 10^{15}$
EPOXY	3.51	3.45	$2.7 \cdot 10^{15}$
PEEK	2.99	1.38	$7.3 \cdot 10^{15}$

This is the accepted version of an article published in IEEE transactions on dielectrics and electrical insulation
DOI: 10.1109/TDEI.2019.008087

4.3 AC BREAKDOWN STRENGTH RESULTS

Experimental AC BDS results are presented in Figure 6. The results demonstrate that the increase of elastic modulus results in a reduced BDS. The effect of the contact pressure is also discernible such that increase of contact pressure by a factor around 3 elevates the interfacial BDS by a factor of 1.4 in the case of the lowest elastic modulus (SiR-SiR) whereas that for the highest modulus (PEEK-PEEK) becomes 2.4 times higher.

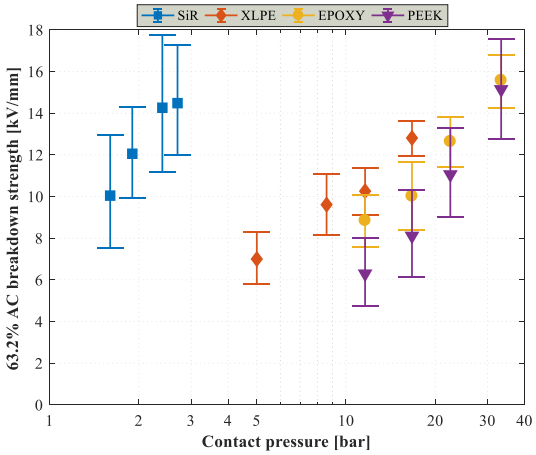

Figure 6. Experimental results of the 63.2% BDS (of 8 single measurements) with the 90% confidence intervals (CI) vs. the contact pressure.

5 DISCUSSION

5.1 ON THE EXPERIMENTAL AC BDS RESULTS

The experimental BDS results indicate that the elastic modulus is one of the prominent material properties affecting the BDS of polymer interfaces. It is observed that materials with lower moduli such as the SiR and XLPE yield higher interfacial BDS values even at lower contact pressures. These findings might sound counter-intuitive at first glance because the model proposed in Section 2.3 predicts a breakdown strength proportional to the fourth root of the elastic modulus.

The previous studies also suggest improved electrical insulating properties when the modulus is increased by adding fillers [12, 13]. It should be highlighted that the model proposed in Section 2.3 stands for the breakdown of bulk insulation (i.e., contact spots). These results accord well with both the experimental and estimated results. Experimental results indicated that materials with lower moduli yield higher interfacial BDS values. Similarly, the electrical tracking resistance model in Equation (6) predicts a breakdown strength proportional to the fourth root of elastic modulus. To sum up, the contact spot breakdown model stands for the breakdown of the bulk insulation along the discharge path.

5.2 ON THE CORRELATIONS BETWEEN THE EXPERIMENTAL AND ESTIMATED RESULTS

In this section, the estimated results by the model are discussed with reference to the instants indicated in Figure 3. First, the average cavity sizes d_{avg} are calculated with their standard deviation (equivalent to 90% CI) and are shown with the hatched regions in Figure 7 while the markers signify the experimentally applied pressure values for reference. Subsequently, the 63.2% BDS and the mean CDIE at the same contact pressures are combined in a single plot in Figure 8 versus elastic modulus. Then, by substituting the min. and max. d_{avg} values in Equation (4), the estimated CDIE values are determined with the CIs thereof. The CDIE versus experimental BDS is plotted in Figure 9. As seen, both the BDS and CDIE are inversely proportional to E'.

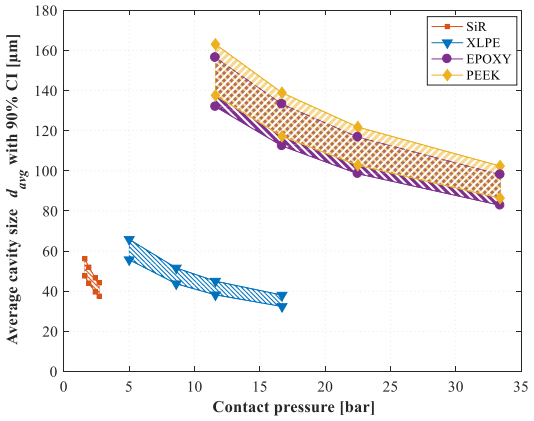

Figure 7. Calculated mean cavity size via Equation (1) vs. contact pressure. Two-sigma significance is utilized to calculate the 90% CI by using the standard deviation of the asperity radius σ_p.

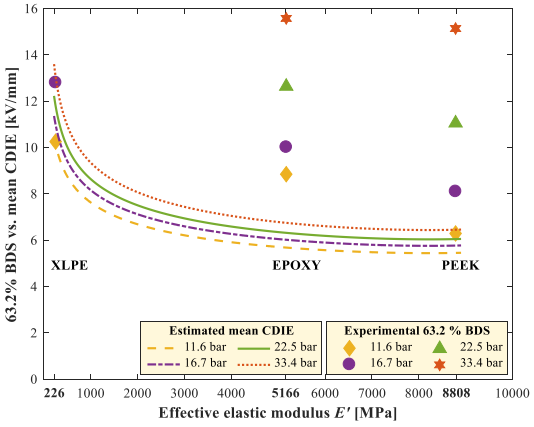

Figure 8. 63.2 % BDS data and mean estimated CDIE vs. elastic modulus for XLPE, EPOXY and PEEK. Contact pressures above 16.7 bar were infeasible due to deformation of the XLPE samples. Similarly, the SiR could not be covered under the same contact pressure.

As seen in the graphs, the BDS of a relatively soft interface, such as SiR-SiR or XLPE-XLPE, indicates a strong correlation with the cavity discharge within the covered pressure range. The ratio of the 63.2% BDS to the mean CDIE is around 0.8−1.2, suggesting that the interfacial breakdown phenomenon is likely to be governed by the cavity discharge in the case of SiR and XLPE. Nevertheless, hard materials studied in this paper, viz. EPOXY and PEEK, exhibited a weaker link between the cavity discharge and the interface breakdown, especially toward relatively higher contact pressures. It can be inferred that the interfacial breakdown phenomenon is not directly controlled by the discharge of vented air-filled cavities at higher elastic modulus, particularly toward high contact pressures. Evidently, the electrical insulating properties of the materials play an essential role in determining the endurance of the contact regions against interfacial discharge.

This is the accepted version of an article published in IEEE transactions on dielectrics and electrical insulation
DOI: 10.1109/TDEI.2019.008087

Figure 10 compares the estimated local field enhancements at the edges of the discharged cavities E_{enh} along with the estimated PD resistances E_{tr} of the studied polymers. Following the convention in Figure 3, instant I stands for the inception of discharge in the averaged-sized cavities whereas instant II represents the moment when the contact spots succumb to the intense local fields caused by the discharged cavities and breakdown. E_{tr} values are estimated via Equation (6) while E_{enh} values are estimated as follows. For the instant I, the mean estimated CDIE values (see Figure 8) are multiplied by the nominal dielectric thickness of 4 mm and are then substituted for V_{app} in Equation (5) along with the mean value of the calculated l_{avg} from Equation (3b). A graph similar to Figure 7 for l_{avg} is available in [11]. Similarly, for the instant II, the experimental BDS values multiplied by 4 mm are substituted for V_{app}.

When discharge activity starts in the cavities in the case of XLPE at the instant I, the enhanced fields at the edges of the contact spots are higher than the electrical tracking resistance that causes local electronic breakdown and bond scission [6]. Thus, the growth rate of the BD channel is further speeded up that eventually leads to an interfacial discharge [6]. At the instant II, the estimated local fields are already higher than the PD resistance of the XLPE. Until the cavity discharge inception, presumably no stress arises at the contact spots according to the average-sized cavity model in the case of XLPE, and once the cavities are discharged, the low PD resistance of XLPE cannot withstand the enhanced local fields and lead to an interfacial discharge. The clear correlation between the cavity discharge and the interface BD in the case of XLPE is further supported by the relation between the PD resistance and the enhanced fields.

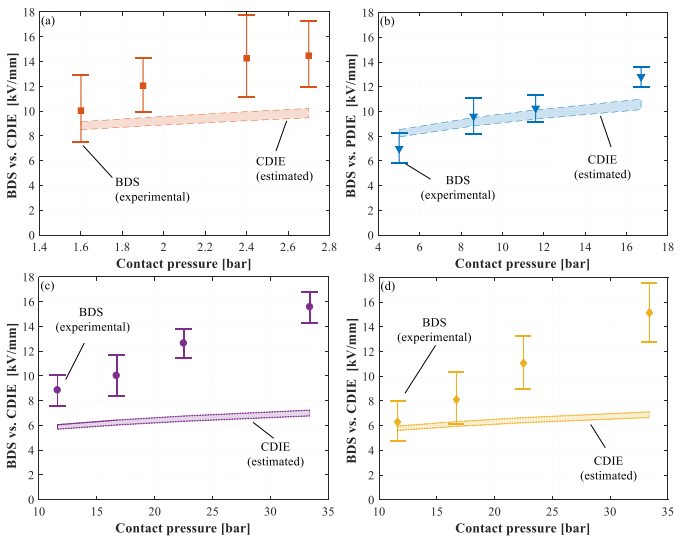

Figure 9. Experimental BDS data (error bars) vs. estimated CDIE (Shaded areas) vs. contact pressure: (a) SiR. (b) XLPE. (c) EPOXY. (d) PEEK.

On the other hand, at the instant I, the enhanced local fields are not high enough to overcome the PD resistances in the case of the EPOXY and the PEEK. Although the average-sized cavities are assumed discharged, high PD resistances of these materials can seemingly withstand the high local fields. At the instant II; however, the enhanced fields exceed the PD resistances of the EPOXY and the PEEK as occurred in the executed BD experiments. These findings shed light on the cause of the low correlation between the cavity discharge and the interface BD in the case of EPOXY and PEEK. It is thus fair to claim that the PD resistance is also a governing insulation property in the interfacial BD phenomenon. As a final remark on the modeling of PD resistance and the enhanced fields: The proposed model is one of the many valid and endorsed theories that are postulated to come up with a plausible account of the observations from real experiments. The assumptions naturally incorporate uncertainties, and the values might deviate from model to model.

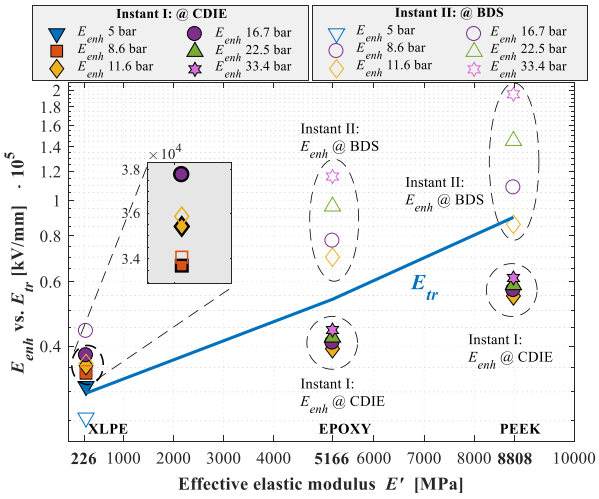

Figure 10. Enhanced field E_{enh} vs. PD resistance E_{tr} within the covered p_a for each interface: Instant I: Cavity discharge inception. Instant II: Breakdown of contact spots. (ε_r = 2.3, G = 20000 J/m^2 and r = 0.3 μm for the XLPE; ε_r = 4.6, G = 20000 J/m^2 and r = 0.3 μm for the EPOXY; and ε_r = 2.8, G = 20000 J/m^2 and r = 0.12 μm for the PEEK [2, 6].)

5.3 LIMITATIONS OF THE PROPOSED MODEL

- The proposed contact surface model simplifies the three-dimensional morphology (3-D) of the surface asperities into two-dimensional cavities and contact spots, which is traversed by the tangential/parallel electric field component. However, cavities are likely to be continuous and connected in 3-D. As a result, the pressure inside the cavities is assumed equal to the ambient pressure and vented cavities are assumed to govern the cavity discharge mechanism.
- Using different materials with different moduli to vary the elastic modulus parameter changes other electrical insulating properties in addition to PD resistance. However, they are not taken into account in the model.
- Non-homogeneous fields at the terminals of a discharged cavity are emulated with a needle-needle electrode pair.

Comments on possible improvements: Due to normally distributed asperity peaks and heights, there are at least some cavities larger than the average-sized cavities, in which the PD activity presumably commences first while there is still no PD activity in the average-sized cavities. Thereby, depending on the number and size of larger cavities, accuracy of the estimated CDIE might dwindle. Consequently, an improved contact model that incorporates the influence of the size and number of the largest cavities might perform better.

This is the accepted version of an article published in IEEE transactions on dielectrics and electrical insulation
DOI: 10.1109/TDEI.2019.008087

5.4 ADDITIONAL ANALYSES

The main aim of this section is to verify the assumptions made in the models in Section 0 by providing additional experimental PD tests. Figure 11 shows the set-up for the PD inception field detection. The setup incorporates an AC (50 Hz) high voltage supply, a test object, a 100-pC-coupling capacitor, and an Omicron MPD 600 equipment, which is connected to a personal computer via fiber optic cables. The system noise was lower than 100 fC, and the PD detection threshold was set to 0.5 pC during tests, which is the PD sensitivity of the system. The time resolution of PD patterns is less than 2 ns, which renders the detected discharge pulse very accurate. For a fair comparison between the BDS and PD tests, the same type of AC voltage ramp of 1 kV/s is applied as performed in the breakdown tests. Four virgin pairs of samples used in each experiment. Each pair was tested three times with five-minute breaks in between.

Firstly, to verify the assumption of needle electrode approach to emulate the field enhancements at the edges of the contact spots, a simple experimental study was designed. Two PEEK samples were prepared as explained in the methodology section. A 1-mm-cylindrical cavity was pierced at the surface of one of the samples (see Figure 12a) to initiate the PD activity at a lower voltage without having the interfacial breakdown immediately [11]. As shown in Figure 12b, the discharged cavity yielded an average PD magnitude around 250 pC until when the PD resistance of the insulation as well as smaller air-filled cavities were overcome by a much higher discharge peak of 13 nC, which is much higher and is probably attenuated due to PD acquisition unit's bandwidth [11].

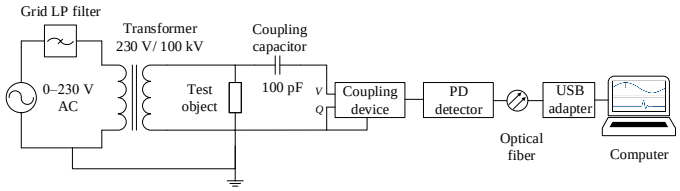

Figure 11. PD test set-up diagram. Coupling device stands for a quadrupole, which is an external measuring impedance for partial discharge measurements.

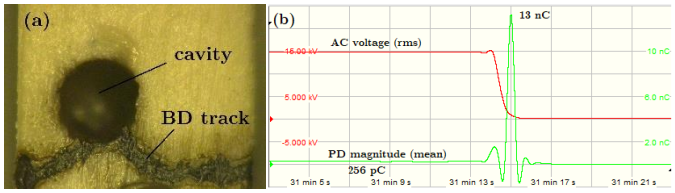

Figure 12. (a) PEEK sample with a cylindrical cavity of 1–mm diameter. (b) PD magnitude vs. applied AC voltage across the polymer interface containing the cavity.

This work is structured such that tangential BDSs are measured, and the cavity discharge inception fields–CDIEs are estimated analytically. The reason why the breakdown testing is favored over the PD testing is as follows: The proposed contact surface model simplifies the three-dimensional morphology of the surface asperities into the two-dimensional profile, which is traversed by the tangential/parallel electric field component. When experimentally measuring the PD inception field (PDIE), it is unclear if the measured data stands for the PDIE of discharged cavities parallel to the electric field (that would cause the imminent interface BD) or for much larger connected cavities not parallel to the field (that is unable to bridge the electrodes). Due to this uncertainty, we performed BDS measurements to ensure that the broken down part of the interface is caused by the discharged cavities parallel to the electric field (see Figure 12a). However, to check the validity of the assumptions made for the theoretical models, some of the experiments performed for the BD testing were repeated to measure the PDIE of the interfaces. To eliminate any ambiguity, we highlight that CDIE denotes the analytically estimated cavity discharge field whereas PDIE stands for the experimentally obtained PD field.

The PD tests of PEEK-PEEK and XLPE-XLPE interfaces were executed to check if the experimental PDIE correlates with the estimated CDIE and experimental BDS values. The PD clusters were verified if the source of the PD is the air-filled cavities at the interface, as they were concentrated near the voltage zero crossing points [10]. The graphs in the first row of Figure 13 show the experimentally obtained PDIE results using the cumulative unreliability of Weibull distribution. Figure 13a indicates that 63.2% PDIE in the case of XLPE is higher than that of the PEEK at 11.6 bar by a factor of 2.3. Increased pressure from 11.6 bar to 22.5 bar has also increased the 63.2% PDIE by a factor of 1.8. Figure 13b shows the comparison of the experimental PDIE and BDS of the XLPE-XLPE interface. The difference between the 63.2% BDS and PDIE is only 10%, which strongly supports the discussion in the previous section that the PD activity in the XLPE evolves to a complete BD right away because the PD resistance of the contact spots cannot withstand the enhanced field for a long time. In contrast, the difference between the 63.2% PDIE and BDS in the case of PEEK-PEEK interface is not as small, i.e., around 55% as seen in Figure 13c at both the contact pressures. Apparently, the contact spots in PEEK could withstand the discharged cavities longer. The performed PD analyses strongly agree with the hypothesis that the PD resistance of the material is an essential insulation property in the interfacial BD phenomenon.

The graphs in the second row of Figure 13 provide additional quantitative PD examination. The PD data was exported to MATLAB and was further processed as explained in [11]. Figure 13d shows that the number of PDs per cycle is the highest in the case of the PEEK, and it further increases at a higher contact pressure. Most discharges occur at the rising edge of the voltage whereas fewer discharges occur at the end of the falling edge of the applied voltage since the electron generation rate is higher at the rising edge [10]. In contrast, the mean charge magnitude in Figure 13e is higher in the second (90°-180°), and fourth quadrants (270°-360°) since fewer PDs per cycle occur in those regions. Overall, XLPE has higher mean charge amplitude. In Figure 13f, the total charge amplitudes per cycle have skewed distributions because a higher number of PDs occurs at the rising edge than at the peak.

6 CONCLUSION

The essential findings from the performed experimental and theoretical studies are listed as follows:

- PD activity in the cavities and electrical tracking resistance of contact spots in series with the cavities are found to be controlling the interfacial breakdown phenomenon.

This is the accepted version of an article published in IEEE transactions on dielectrics and electrical insulation
DOI: 10.1109/TDEI.2019.008087

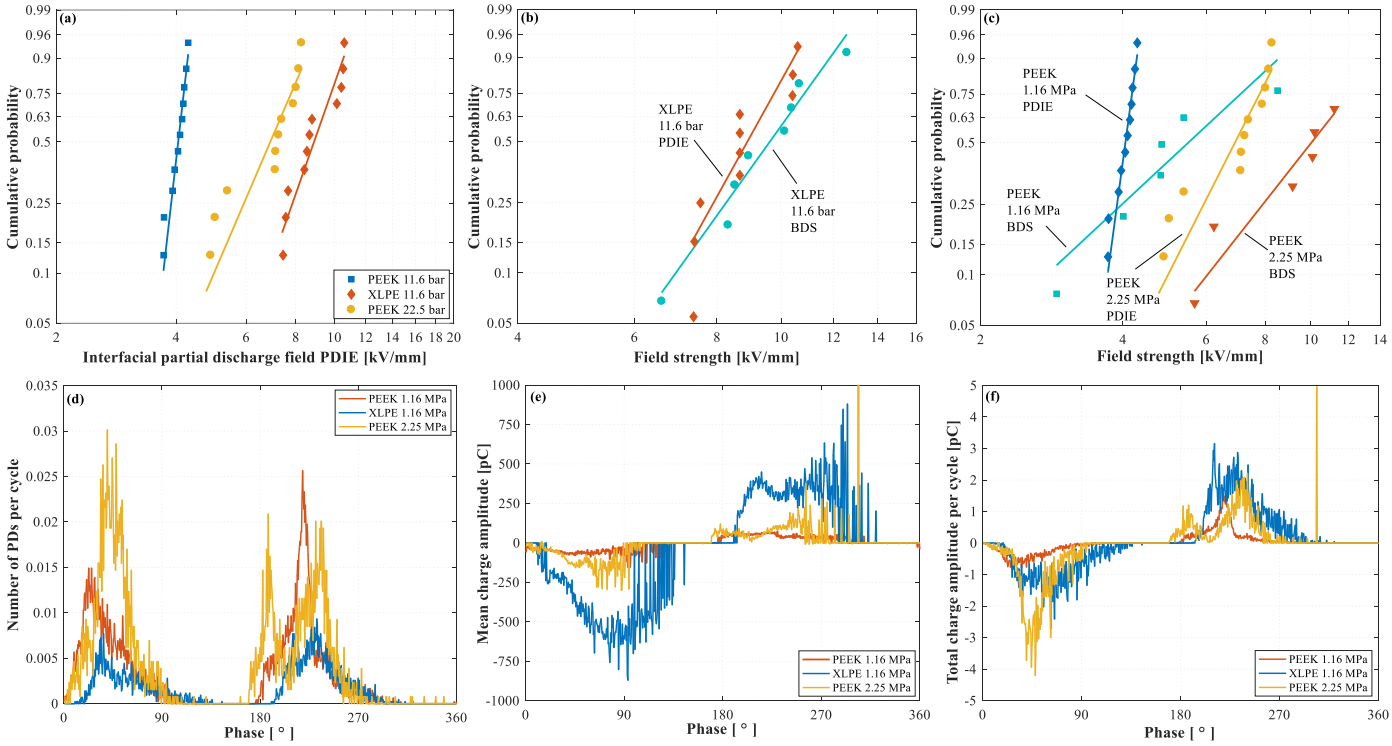

Figure 13. (a) PDIE of XLPE and PEEK. (b) Experimental PDIE vs BDS of XLPE. (c) Experimental PDIE vs. BDS of PEEK. (d) Number of PDs per cycle vs. phase angle. (e) Mean charge amplitude vs phase angle. (f) Total charge amplitude per cycle vs. phase angle.

- Both the analytically estimated cavity discharge inception field and the experimentally determined breakdown strength decrease at higher elastic modulus. Performed PD inception field tests also provided parallel results.
- The proposed models suggest that increase of elastic modulus reduce the dominance of the discharged cavities over the interfacial breakdown phenomenon while increasing the governance of electrical tracking resistance. At higher contact pressures, the difference between these mechanisms becomes more discernible.
- To our knowledge, the proposed theoretical model is novel in incorporating diverse interdisciplinary fields to model interface breakdown between polymers. As a result of the reasonable agreement between the estimated results and experimental results, we believe that the model deserves further attention.

ACKNOWLEDGMENT

This work is funded by the project "High Voltage Subsea Connections (SUBCONN)." The project is supported by The Research Council of Norway (Project No. 228344/E30).

REFERENCES

[1] E. Peschke and R. von Olshausen, *Cable systems for high and extra-high voltage: development, manufacture, testing, installation, and operation of cables and their accessories*, Wiley-VCH, 1999.

[2] L. A. Dissado and J. C. Fothergill, "Electrical degradation and breakdown in polymers," IET, 1992, vol. 9.

[3] B. X. Du, J. G. Zhang, and D. S. Liu, "Interface charge behavior of multi-layer oil-paper insulation under DC and polarity reversal voltages," IEEE Trans. on Dielectr. Electr. Insul., vol. 22, no. 5, pp. 2628–2638, Oct. 2015.

[4] J. H. Mason, "Assessing the resistance of polymers to electrical treeing," IEE Proc. A – Phys. Sci., Meas. Inst. Man. Edu. - Reviews, vol. 128, no. 3, pp. 193–201, Apr. 1981.

[5] X. Chen, Y. Xu, X. Cao, and S. M. Gubanski, "Electrical treeing behavior at high temperature in XLPE cable insulation samples," IEEE Trans. Dielectr. Electr. Insul., vol. 22, no. 5, pp. 2841–2851, 2015.

[6] J. C. Fothergill, "Filamentary electromechanical breakdown," IEEE Trans. Electr. Insul., vol. 26, no. 6, pp. 1124–1129, 1991.

[7] R. M. Eichhorn, "Treeing in Solid Extruded Electrical Insulation," IEEE Trans. Electr. Insul., vol. EI-12, no. 1, pp. 2–18, 1977.

[8] B. Bhushan, "Contact mechanics of rough surfaces in tribology: multiple asperity contact," Tribology Letters, vol. 4, no. 1, pp. 1–35, 1998.

[9] E. Kantar, S. Hvidsten, F. Mauseth, and E. Ildstad, "A stochastic model for contact surfaces at polymer interfaces subjected to an electrical field," Tribology Int., vol. 127, pp. 361–371, 2018.

[10] H. Illias, G. Chen, and P. L. Lewin, "Modeling of partial discharge activity in spherical cavities within a dielectric material," IEEE Electrical Insul. Mag., vol. 27, no. 1, pp. 38–45, 2011.

[11] E. Kantar, "Characterization of Longitudinal AC Electric Breakdown Strength of Solid Dielectric Interfaces," Ph.D. dissertation, Norwegian University of Science and Technology, 2018.

[12] M. Roy, J. K. Nelson, R. K. MacCrone, L. S. Schadler, C. W. Reed, and R. Keefe, "Polymer nanocomposite dielectrics-the role of the interface," IEEE Trans. Dielectr. Electr. Insul., vol. 12, no. 4, pp. 629–643, 2005.

[13] S. Albayrak, C. Becker-Willinger, M. Aslan, and M. Veith, "Influence of nano-scaled zirconia particles on the electrical properties of polymer insulating materials," IEEE Trans. Dielectr. Electr. Insul., vol. 19, no. 1, pp. 76–82, 2012.

Emre Kantar (M'14) received the B.Sc. and M.Sc. degrees in electrical engineering from Middle East Technical University, Ankara, Turkey, in 2011 and 2014, respectively. He is currently a Ph.D. candidate at the Department of Electric Power Engineering, NTNU in Trondheim, Norway.

Erling Ildstad received the M.Sc. degree in technical physics in 1978 and the Ph.D. degree in electrical power engineering in 1982 from NTNU in Trondheim, Norway. He has been a full-time professor of high voltage engineering at NTNU since 1993.

Sverre Hvidsten received the M.Sc. degree in 1992 at the Norwegian Institute of Technology (NTH) in Trondheim. In 1999, he gained the Ph.D. in electrical engineering at NTNU in Trondheim. Since then, he has been working for SINTEF Energy Research.

This is the accepted version of an article published in IEEE transactions on dielectrics and electrical insulation
DOI: 10.1109/TDEI.2019.008087